2016 NDIA GROUND VEHICLE SYSTEMS ENGINEERING AND TECHNOLOGY SYMPOSIUM
POWER & MOBILITY (P&M) TECHNICAL SESSION
AUGUST 2-4, 2016 - NOVI, MICHIGAN

POWER CAPABILITY AND PROGNOSIS SIMULATION FOR BB-2590 LITHIUM ION BATTERIES ON SMALL UNMANNED GROUND VEHICLES BY SEMI-EMPIRICAL MODEL

Yoichi Takeda Ph.D.
David Skalny
John Zwally
Laurence Toomey Ph.D.
US Army RDECOM-TARDEC
Warren, MI

ABSTRACT

This paper presents a semi-empirical model for predicting capability and life span of small size Lithium ion battery packs. The model consists of a simple Battery Management System (BMS) model, an existing electro-thermal model as well as calendar and cycle aging models. In this work we aimed to realize both fast calculation and high flexibility by using a simplified thermal and cycle aging model with Rainflow method, a method usually used for evaluating material fatigue. This paper details the mathematical structure of the model. The methodology is applied to a $LiCoO_2$/carbon BB-2590 type battery pack utilized for small Unmanned Ground Vehicles. Moreover, simulation results of a capability test of an on-board battery, a 10 year calendar life test and a cycle test with 500 charging and discharging cycles are shown.

1. Introduction

Battery-driven small Unmanned Ground Vehicles (UGVs) are frequently used by the U.S. Army for missions such as explosive ordinance disposal, demining and surveillance. In these UGVs, power consumption is a paramount factor in limiting the mission length as well as robotic capability. Accordingly, maximization of usable capacity as well as reduced capacity and power fade are especially important for small UGV batteries. Current UGVs, such as the iRobot Packbot, typically utilize BB-2590 Li ion batteries instead of proprietary batteries in order to ease logistical concerns, save money and increase energy density over lead acid alternatives. The BB-2590 is a battery pack with 18650 cylindrical $LiCoO_2$/carbon cells which is quite widely utilized for man portable communication and information technology equipment within the U.S. Department of Defense. As this battery is primarily designed for man portable C4I equipment, use in robotic applications results in unique effects on battery life and performance due to different power profiles and usage environments from assumed original conditions. An effective approach for maximizing the useable capacity and life of the battery is development of a power and energy management strategy considering fundamental physical and chemical phenomena. One of the well-known methods for developing such strategies is utilizing semi-empirical models. However, existing strategies for small UGVs currently do not take into consideration these fundamental aspects. To develop such strategies, we made a semi-empirical model for small robotic batteries and simulated capacity, age and health under some typical situations.

The electric properties and thermal characteristics of individual batteries affect capability and life of battery system. However, it is difficult to depict the whole effect due to complexity of physical and chemical mechanisms. In order to predict and real-time estimate capability and life of Li ion battery cells, many semi-empirical battery models have been described in literature over the last decade [1]-[6]. However, reports for semi-empirical models for whole battery pack system life are sparse. Especially for cycle degradation, it is difficult to deal with arbitrary working situations because there are few methods for automatically counting cycles. In some of the literature [7], [8], one origin of the capacity and impedance degradation is the swelling and shrinking of active material particles due to intercalation and declaration of Li ions. Therefore, the model [7] included the Wöhler relationship, which is a popular relationship to describe certain repeated stress or strain amplitude and number. Of the methods to express relationships between random strain profiles and material fatigue, the Rainflow method is one general method[9]. In this work, the Rainflow method was adapted to estimate cycle degradation of Li-ion batteries with arbitrary electro-thermal profiles. Another problem is a paradox between fidelity and calculation time. The model minimizes the number of ordinary differential equations and uses a simple heat dissipation model to realize short calculation times. Also, this model can express a battery system with a distribution of battery cell electric properties, capacities, impedance and leakage currents.

This paper proposes a systematic modeling and simulation methodology to easily predict the capability and prognosis for on-board small battery packs and shows simulation results of the model under various situations.

This paper is organized as follows. Section 2 introduces the mathematical approach used for the electro-thermal and aging models for small battery packs utilized in UGVs. Section 3 describes parameter acquisition for the BB2590 battery. Section 4 shows simulation data under some typical situation and discusses the usefulness of the methodology.

2. Electrical-thermal model and aging model

In this section, a combined electro-thermal and aging model is formulated for small battery packs with cylindrical battery cells. Physical specifications of these battery cells in a pack, which are leak electric current I_{leak}, Ohmic resistance R_{zs} and capacity of cells CAP_{cell} have distributions derived with manufacturing process. A battery pack composed of n series connected super

Nomenclature

C: capacitance [F]
$\mathcal{C}$: heat capacitance [JK^{-1}]
CAP: battery capacity [Ah]
E_a: activation energy [J]
F: Faraday constant 96485[Cmol^{-1}]
I: electric current [A]
N: number of battery cells in the battery pack
P: thermal resistance [KW^{-1}]
R: electric resistance [Ohm]
$\mathcal{R}_{ug}$: universal gas constant 8.3145 [J K^{-1} mol^{-1}]
SoC: state of charge
T: temperature [K]
$\bar{T}$: volume averaged temperature of the battery cell [K]
$\mathcal{T}_k$: elapsed time by the end of kth peak or valley of $\Delta DOD + \phi C - rate$ curve [sec]
V: voltage [V]
W: volume [m^3]
c_p: specific heat coefficient [J kg^{-1} K^{-1}]
h: Convection coefficient [W/m^{-2}K^{-1}]
k_t: Thermal conductivity [W/mK^{-1}]
$\dot{q}$: Joule heat [J]
r: radius of battery cell [m]
t_{pv}: Time between peak and valley of the $\Delta DOD + \phi C - rate$ curve [sec]

Greek characters
α: differentiated V_{oc} with respect to SoC when time is t [Vsec^{-1}]
$\bar{\gamma}$: volume averaged temperature gradient [Ksec^{-1}]
υ: cycle number
ρ: density [kgm^{-3}]
τ: time [sec]
Δt: interval time between observing opportunity [sec]
ΔDOD: the difference of 1-SoC between peak and valley of the the $\Delta DOD + \phi C - rate$ curve

Subscripts
amb: ambient
cal: calendar fade
cc: center of the cell
$cell$: battery cell
cyc: cycle fade
$leak$: leak current
$nominal$: the value which used parameter acquisition
oc: open circuit
$pack$: battery pack
sc: surface of the cell
sp: surface of the pack
$supercell$: supercell
t: specific observing time
zs : ohmic resistance content in equivalent circuit
$z1$: first RC content in equivalent circuit
$z2$: second RC content in equivalent circuit
C: capacity of a battery cell
R: ohmic resistance components of equivalent circuit of a battery cell

cells with m parallel connected cells is shown in Figure 1. The terminal voltage is described by an equivalent circuit and three-state heat dissipation model which estimates temperature of battery cells' cores and surfaces and the surface of a battery pack. As for the equivalent circuit, its components, resistance and capacitance, are varied by temperature of the battery cells' core temperatures, state of charge (SoC) as well as calendar and cycle life factors. The calendar and cycle life factors are described by the model reported by Smith et al.[7]. However, to adapt the reported model to various situations containing arbitrary real-time electric signals, we added a c-rate factor and utilized the Rainflow method. The Rainflow method is a well-known method to estimate material fatigue with random stress.

2.1 Electrical model

The schematic of the equivalent circuit model is shown in Figure 2. The input signal to the model is electric current or voltage applied to a battery pack. The ohmic resistance of the circuit: R_{zs} can be expressed as a function of temperature of the battery cell. The center of the cell temperature $T_{cc}(\tau)$ is utilized for representing value of the cell temperature. The other components of the circuit R_{z1}, C_{z1}, R_{z2} and C_{z2} shown in Figure 2 can be expressed as the function of $SoC(\tau)$ and $T_{cc}(\tau)$. However, the variation of these components is negligible because the Shift amount of these values are slow enough in interval time compared to the electric property measurement of batteries. The difference equations method is utilized to obtain electric specifications such as voltage and electric current. The method doesn't need large matrix calculation and uses ordinary difference equation solvers.

Where discharge current is defined as positive, the voltage of equivalent circuit $V_{cell}(\tau)$ can be presented by

$$V_{cell}(\tau) = V_{oc}\big(SoC_{cell}(\tau)\big) - V_{zs}\big(T_{cc}(\tau), I_{cell}(\tau)\big) - \sum_{l=1}^{2} V_{zl}(SoC_{cell}(\tau), T_{cc}(\tau), I_{cell}(\tau)) \quad (l = 1\ or\ 2) \tag{1}$$

where $I_{cell}(\tau)$ is the sum of leakage current I_{leak} and electric current through the battery cell. V_{oc} is the open circuit voltage of the battery cell. V_{zs} and V_{zl} are voltage of components in equivalent circuit shown in Figure 2. The value of SoC is also calculated by Coulomb counting as

$$\frac{dSoC_{cell}(\tau)}{d\tau} = -\frac{1}{3600CAP_{cell}} I_{cell}(\tau) \tag{2}$$

In this equation, CAP_{cell} is regarded as constant though it is function of time. The reason is because $CAP_{cell}(\tau)$ is only changed by aging phenomena in this model. The reduction of $CAP_{cell}$by aging is negligible in measurement time interval as it is as short as several dozen seconds. The second term of Equation (1) is the voltage as a function of ohmic resistance. It is represented by

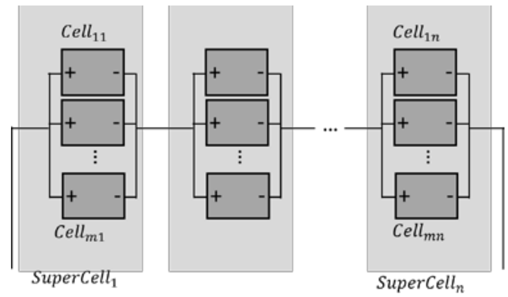

Figure 1. Schematic of a battery pack with *n* series connected supercells which include *m* parallel connected battery cells.

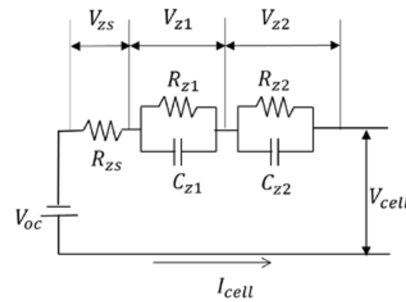

Figure 2. Schematic of equivalent circuit for battery cells.

$$V_{zs}(\tau) = R_{zs}I(\tau) \tag{3}$$

The third term of Equation (1), the V_{zl} is described as

$$\frac{dV_{zl}(\tau)}{dt} = \frac{1}{R_{zl}C_{zl}}V_l(\tau) + \frac{1}{C_{zl}}I(\tau) \quad (l = 1\ or\ 2) \tag{4}$$

where R_{zl}, C_{zl} are equivalent resistance and capacitance, respectively. These R_{zl}, C_{zl} values are fitted to a function of cell core temperature, T_{cc} and $SoC[1]$. Both T_{cc} and SoC are a function of time. If we prepare discrete data points for electric current $I(\tau)$, $V(t)$ can be represented by difference equations instead of ordinary differential equations to save computational resources. We approximated a random electric current by the summation of the step functions shown as follows.

$$I_{cell}(\tau)_{\tau=t} \equiv I_{cell,t} = \sum_{k=-(n-1)}^{0} \big(I_{cell,t+k\Delta t} - I_{cell,t+(k-1)\Delta t}\big)u(t - k\Delta t) \tag{5}$$

where $u(t)$ is the unit step function and $t - n\Delta t$ is equal to 0. Δt is the time interval between discrete step. Next we explain the discrete expression of the cell voltage $V_{cell}(\tau)$. Before establishing the difference equation of Equation (1), the discrete

SoC should be shown. The integrated discrete SoC is described by expanded Equation (2) as

$$SOC_{cell}(\tau)_{\tau=t} \equiv SoC_{cell,t} = SoC_{cell,0} - \int_0^t \frac{1}{3600CAP_{cell}} I_{cell}(\tau)d\tau$$
$$\cong SoC_{cell,0} - \sum_{k=-(n-1)}^{0} \frac{1}{3600CAP_{cell}} I_{cell,t+k\Delta t}\Delta t \quad (6)$$

Thus the difference equation of $SoC_{cell,t}$ is described as

$$SoC_{cell,t} = SoC_{cell,t-\Delta t} - \frac{1}{3600CAP_{cell}} I_{cell,t}\Delta t \quad (7)$$

In the first term of Equation (1), V_{oc} is defined as

$$V_{oc,t} \equiv \alpha_t SoC_{cell,t} + V_{oc,t-\Delta t} \quad (8)$$

Inserting Equation (7) into Equation (8) makes the difference equation for $V_{oc,}$, which is described as

$$V_{oc,t} = V_{oc,t-\Delta t} - \frac{\alpha_t}{3600CAP_{cell}} I_{cell,t}\Delta t \quad (9)$$

Where α_t is the value of differentiated $V_{oc,t}$ with respect to SoC. α_t can analytically be obtained by Equation (38) in Section 3. 1. By inserting Equation (5) into Equation (3), $V_{zs,t}$ can be found as follows.

$$V_{zs,t} = R_{zs,t} I_{cell,t} \quad (10)$$

To describe V_{zl} by difference function, we use Laplace transform and inverse Laplace transform as shown in the following calculations. The Laplace transform of Equation (4) is expressed as

$$V_{zl}(s) = \frac{\frac{1}{R_{zl}C_{zl}}}{s\left(s + \frac{1}{R_{zl}C_{zl}}\right)} R_{zl} I_{cell}(s) \qquad (l = 1 \; or \; 2) \quad (11)$$

By inserting the Laplace transform of Equation (5) into Equation (11), Equation (11) is expanded as

$$V_{zl,t}(s) = \sum_{k=-(n-1)}^{0} \frac{\frac{1}{R_{zl,t+k\Delta t}C_{zl,t+k\Delta t}}}{s\left(s + \frac{1}{R_{zl,t+k\Delta t}C_{zl,t+k\Delta t}}\right)} R_{zl,t+k\Delta t}\big(I_{cell,t+k\Delta t} - I_{cell,t+(k-1)\Delta t}\big) e^{-(k+n)\Delta ts} \quad (l = 1 \; or \; 2) \quad (12)$$

Moreover, inverse Laplace transformation of Equation (12) is described as

$$V_{zl,t} = \sum_{k=-(n-1)}^{0} R_{zl,t+k\Delta t}\left(I_{cell,t+k\Delta t} - I_{cell,t+(k-1)\Delta t}\right) \left(1 - e^{-\frac{1}{R_{l,t+k\Delta t}C_{l,t+k\Delta t}}t}\right) u(t)\delta(t-(k+n)\Delta t)$$
$$= \sum_{k=-(n-1)}^{0} R_{zl,t+k\Delta t}\left(I_{cell,t+k\Delta t} - I_{cell,t+(k-1)\Delta t}\right) \left[1 - e^{-\frac{1}{R_{zl,t+k\Delta t}C_{zl,t+k\Delta t}}(t-(n+k)\Delta t)}\right] \qquad (l = 1 \; or \; 2) \quad (13)$$

where δ represents Kronecker delta. By expanding Equation (13) the difference Equation of $V_{l,t}$ is obtained as

$$V_{zl,t} = R_{zl,t-\Delta t} I_{cell,t-\Delta t}\left(1 - e^{-\frac{\Delta t}{R_{zl,t-\Delta t}C_{zl,t-\Delta t}}}\right) + e^{-\frac{\Delta t}{R_{zl,t-2\Delta t}C_{zl,t-2\Delta t}}} V_{zl,t-\Delta t} \qquad (l = 1 \; or \; 2) \quad (14)$$

In Equation (14), $R_{zl,t-2\Delta t}$ and $C_{zl,t-2\Delta t}$ are regarded as the same value of $Rz_{l,t-\Delta t}$ and $C_{zl,t-\Delta t}$, respectively. Thus, Equation (1) can be expanded by Equations (9), (10) and (14) as

$$V_{cell,t} = V_{oc,t-\Delta t} - \frac{\alpha_t}{3600CAP_{cell}} I_{cell,t}\Delta t - R_{zs,t} I_{cell,t} - \sum_{l=1}^{2}\left[R_{zl,t-\Delta t} I_{cell,t-\Delta t}\left(1 - e^{-\frac{\Delta t}{R_{zl,t-\Delta t}C_{zl,t-\Delta t}}}\right) + e^{-\frac{\Delta t}{R_{zl,t-\Delta t}C_{zl,t-\Delta t}}} V_{zl,t-\Delta t}\right] \quad (15)$$

This equation shows the external voltage of a battery cell of the electric model.

As the next step, a battery pack composed n series connected super cells with m parallel connected cells as shown in Figure 2 is considered. The BB-2590 is composed of eight series supercells which have three parallel cells. In this case, the relationship between the electric current and voltage of the battery pack, super cells and battery cells can be described as

$$I_{pack} = I_{supercell,j} = \sum_{i=1}^{m} I_{cell,ij} \quad (16a)$$

$$V_{pack} = \sum_{j=1}^{n} V_{supercell,j} \quad (16b)$$

$$V_{supercell,j} = V_{cell,ij} \quad (16c)$$

Where, I_{pack} is the input signal of the electrical model of a battery pack. V_{pack} is the voltage of the whole battery pack. $I_{supercell,j}$ and $V_{supercell,j}$ are the electric current and voltage of jth supercell, respectively. Next, the method to obtain electric current of each cells in a supercell is shown. The voltage of jth supercell can be described utilizing Equation (15) and Equations (16) by

$$V_{ij} = V_{supercell,i,t} = -A_{ij,t} I_{cell,ij,t} + B_{ij,t} \quad (17a)$$

$$A_{ij,t} = \frac{\alpha_{ij,t}}{CAP_{cell,ij}}\Delta t + R_{zs,ij,t} \quad (17b)$$

$$B_{ij,t} = V_{oc,ij,t-\Delta t} - \sum_{l=1}^{2}\left[R_{zl\,ij,t-\Delta t} I_{cell,ij\,t-\Delta t}\left(1 - e^{-\frac{\Delta t}{R_{zl\,ij,t-\Delta t} C_{zl\,ij,t-\Delta t}}}\right) + e^{-\frac{\Delta t}{R_{zl\,ij,t-\Delta t} C_{zl\,ij,t-\Delta t}}} V_{zl\,ij,t-\Delta t}\right] \tag{17c}$$

The $I_{cell,ij,t}$ can expressed by expanded Equations (16) and (17) as

$$I_{cell,ij,t} = \frac{B_{ij,t}\sum_{i=1}^{m}\frac{1}{A_{ij,t}} + I_{pack,t} - \sum_{i=1}^{m}\frac{B_{ij,t}}{A_{ij,t}}}{A_{ij,t}\sum_{i=1}^{m}\frac{1}{A_{ij,t}}} \tag{18}$$

In Equations (17), $I_{cell,ij,t}$ and all variables with subscripts $t-\Delta t$ are known values at time . On the other hand, $R_{zs,ij,t}$ $\alpha_{ij,t}$ are unknown values at time . Therefore, A self-consistent calculations between Equations (17) and (18) are conducted in this model. To calculate $I_{cell,ij,t}$ of time "t", $R_{zs,ij,t-\Delta t}$, $\alpha_{ij,t-\Delta t}$ are inserted in the Equation (17) instead of $R_{0\,ij,t}$ $\alpha_{ij,t}$. Through Equations (7), (17) and (18), $I_{cell,ij,t}$, $SoC_{cell,ij,t}$ $\alpha_{ij,t}$ and $R_{zs,ij,t}$ are obtained. By inserting those obtained values into Equation (17) again and re-calculating Equations (17) and (18), a more accurate $I_{ij,t}$ is obtained. As far as our conducted calculation, $I_{cell,ij,t}$, $SoC_{cell,ij,t}$, $\alpha_{ij,t}$ and $R_{zs,ij,t}$ are converged within 0.001% error in several recalculations. Moreover, the $SoC_{supercell,t}$are $SoC_{pack,t}$ are defined as

$$SoC_{supercell,i,t} = SoC_{supercell\,i,t-\Delta t} - \sum_{i=1}^{m}\frac{I_{ij,t}}{CAP_{cell,ij}}\Delta t \tag{19a}$$

$$SoC_{pack,t} = \frac{\sum_{j=1}^{n}\left(SoC_{supercell,i,t}\sum_{i=1}^{m} CAP_{cell,ij}\right)}{\sum_{i=1}^{m}\sum_{j=1}^{n} CAP_{cell,ij}} \tag{19b}$$

Moreover, V_{pack} is obtained by Equation (16b).

In the case where of V_{pack} is the input signal, such as constant voltage charging mode, the values of $I_{cell,ij,t}$ should be expressed by $V_{pack,t}$. By expanding Equations (16) and (17), $I_{pack,t}$ is expressed by

$$I_{pack,t} = \sum_{i=1}^{m} I_{ij} = \sum_{i=1}^{m}\frac{B_{ij,t}}{A_{ij,t}} - V_{supercell\,i,t}\sum_{i=1}^{m}\frac{1}{A_{ij,t}} \tag{20}$$

By expanding Equations (16) and (20), $V_{pack,t}$ is expressed by

$$V_{pack,t} = \sum_{j=1}^{n} V_{supercell\,j,t} = -I_{pack}\sum_{j=1}^{n}\frac{1}{\sum_{i=1}^{m}\frac{1}{A_{ij,t}}} + \sum_{j=1}^{n}\frac{\sum_{i=1}^{m}\frac{B_{ij,t}}{A_{ij,t}}}{\sum_{i=1}^{m}\frac{1}{A_{ij,t}}} \tag{21}$$

By inserting expanded Equation (18) to (21), $I_{ij,t}$ is expressed by $V_{pack,t}$, $A_{ij,t}$ and $B_{ij,t}$ as

$$I_{cell,ij,t} = \frac{\left(B_{ij,t}\sum_{i=1}^{m}\frac{1}{A_{ij,t}} - \sum_{i=1}^{m}\frac{B_{ij,t}}{A_{ij,t}}\right)\sum_{j=1}^{n}\frac{1}{\sum_{i=1}^{m}\frac{1}{A_{ij,t}}} - V_{pack,t} + \sum_{j=1}^{n}\frac{\sum_{i=1}^{m}\frac{B_{ij,t}}{A_{ij,t}}}{\sum_{i=1}^{m}\frac{1}{A_{ij,t}}}}{A_{ij,t}\sum_{i=1}^{m}\frac{1}{A_{ij,t}}\sum_{j=1}^{n}\frac{1}{\sum_{i=1}^{m}\frac{1}{A_{ij,t}}}} \tag{22}$$

$SoC_{supercell,t}$, $SoC_{pack,t}$ and V_{pack} are also obtained by Equations (19a), (19b) and (16a), respectively.

2.2 Thermal model

The thermal model of a cylindrical cell in a thermal chamber with evenly distributed heat generation, ignoring the thermal distribution along the positive-negative pole axis, can described as in Equation (23)[10].

$$\frac{d\boldsymbol{x}}{dt} = \boldsymbol{Ax} + \boldsymbol{Bu} \tag{23a}$$

$$\boldsymbol{y} = \boldsymbol{Cx} + \boldsymbol{D} \tag{23b}$$

where $\boldsymbol{x} = [\bar{T}\ \ \bar{\gamma}]^T$, $\boldsymbol{u} = \left[\dot{q}\ \ \ T_{sp}\right]^T$ and $\boldsymbol{y} = [T_{cc}\ \ T_{sc}]^T$ are system status, input and output respectively. $\bar{T}$ and $\bar{\gamma}$ are volume averaged temperature of the cell and volume averaged temperature gradient, respectively. T_{cc} , T_{sc} and T_{sp} are the temperature of center, surface of a battery cell and the surface of a battery pack. System matrix $\boldsymbol{A}$, $\boldsymbol{B}$, $\boldsymbol{C}$ and $\boldsymbol{D}$ can be defined as

$$\boldsymbol{A} = \begin{bmatrix} a_{11} & a_{12} \\ a_{21} & a_{22} \end{bmatrix} = \begin{bmatrix} \frac{-48k_t h}{\rho c_{p,cell} r(24k_t + rh)} & \frac{-15k_t h}{\rho c_{p,cell}(24k_t + rh)} \\ \frac{-320k_t h}{\rho c_{p,cell} r^2(24k_t + rh)} & \frac{-120k_t(4k_t + rh)}{\rho c_{p,cell} r^2(24k_t + rh)} \end{bmatrix} \tag{24a}$$

$$\boldsymbol{B} = \begin{bmatrix} b_{11} & b_{12} \\ b_{21} & b_{22} \end{bmatrix} = \begin{bmatrix} \frac{1}{W_{cell}\rho c_{p,cell}} & \frac{48k_t h}{\rho c_{p,cell} r(24k_t + rh)} \\ 0 & \frac{320k_t h}{\rho c_{p,cell} r^2(24k_t + rh)} \end{bmatrix} \tag{24b}$$

$$\boldsymbol{C} = \begin{bmatrix} c_{11} & c_{12} \\ c_{21} & c_{22} \end{bmatrix} = \begin{bmatrix} \frac{24k_t - 3rh}{24k_t + rh} & -\frac{120rk_t + 15r^2 h}{8(24k_t + rh)} \\ \frac{24k_t}{24k_t + rh} & \frac{15rk_t}{2(24k_t + rh)} \end{bmatrix} \tag{24c}$$

$$\boldsymbol{D} = \begin{bmatrix} d_{11} & d_{12} \\ d_{21} & d_{22} \end{bmatrix} = \begin{bmatrix} 0 & -\frac{4rh}{24k_t + rh} \\ 0 & \frac{rh}{24k_t + rh} \end{bmatrix} \tag{24d}$$

where r and W_{cell} are radius and volume of the battery cell and k_t is the radial direction thermal conductivity of the cell.

Where h shows the heat transfer coefficient, in case a battery cell is bared ambient air. However, the value should be changed in this model because the battery cells are surrounded by battery pack housing and the distance between of housing and battery cells are as short as several millimeters. Therefore the heat conduction between battery cells and pack surface are considered to decide the h value. The generated heat $\dot{q}$ is a byproduct of the chemical reaction occurring in the jelly roll and Joule heat at the electrode during battery operation. The $\dot{q}$ is defined by the electric model as

$$\dot{q} \equiv V_{zs} I_{cell} + \frac{{V_{z1}}^2}{R_{z1}} + \frac{{V_{z2}}^2}{R_{z2}} \tag{25}$$

As for our model, in order to depict the battery pack heat dissipation, Equation (26) is added to Equations (23) .The temperature of battery pack surface or T_{sp} can defined as functions of T_{sc} and T_{amb}.

$$\frac{C_{pack}}{N}\frac{dT_{sp}}{dt} = \frac{T_{amb} - T_{sp}}{P_{pack}} - \frac{T_{sp} - T_{sc}}{P_{cell}} \tag{26}$$

where P_{pack} and P_{cell} are lamped thermal resistance between the surface of the cell and battery pack and between battery pack and ambient. C_{pack} shows the heat capacitance of the battery pack except for the battery cells, including the pack housing and BMS board. In addition N shows number of battery cells in a battery pack. This Equation indicates the approximation of generated heat from each cell dissipated to a specific area of the pack surface like a “window”, which area is equal to the total pack area divided by the number of cells in the pack. The T_{amb}, ambient temperature, is one of the input signal of this model. This value can be replaced by a function such as a sinusoidal day and night temperature variation. T_{sc} is described by $\bar{T}, \bar{\gamma}$ and T_{sp} as

$$T_{sc} = \frac{24k_t}{24k_t + rh}\bar{T} + \frac{15rk_t}{2(24k_t + rh)}\bar{\gamma} + \frac{rh}{24k_t + rh}\, T_{sp} \tag{27}$$

From Equations (26) and (27), the T_{sp} is describes as

$$\frac{dT_{sp}}{dt} = e_1\bar{T} + e_2\bar{\gamma} + e_3\, T_{sp} + e_4 T_{amb} \tag{28a}$$

$$e_1 = \frac{24Nk_t}{C_{pack}P_{cell}(24k_t + rh)} \tag{28b}$$

$$e_2 = -\frac{15Nrk_t}{2C_{pack}P_{cell}(24k_t + rh)} \tag{28c}$$

$$e_3 = -\frac{N}{C_{pack}}\left\{\frac{1}{P_{pack}} + \frac{1}{P_{cell}}\left(1 - \frac{rh}{24k_t + rh}\right)\right\} \tag{28d}$$

$$e_4 = \frac{N}{C_{pack}P_{pack}} \tag{28e}$$

The battery pack thermal model is described by expanded Equations (23), (24) and (28) as

$$\frac{d\boldsymbol{x}'}{dt} = \boldsymbol{A}'\boldsymbol{x}' + \boldsymbol{B}'\boldsymbol{u}' \tag{29a}$$

$$\boldsymbol{y}' = \boldsymbol{C}'\boldsymbol{x}' + \boldsymbol{D}' \tag{29b}$$

where $\boldsymbol{x}' = \begin{bmatrix}\bar{T} & \bar{\gamma} & T_{sp}\end{bmatrix}^T$, $\boldsymbol{u}' = [\dot{q} \;\; 0 \;\; T_{amb}]^T$ and $\boldsymbol{y}' = \begin{bmatrix}T_{cc} & T_{sc} & T_{sp}\end{bmatrix}^T$ are system status, input and output respectively. System matrix $\boldsymbol{A}'$, $\boldsymbol{B}'$, $\boldsymbol{C}'$ and $\boldsymbol{D}'$ can be defined as

$$\boldsymbol{A}' = \begin{bmatrix} a_{11} & a_{12} & b_{12} \\ a_{21} & a_{22} & b_{22} \\ e_1 & e_2 & e_3 \end{bmatrix} \tag{30a}$$

$$\boldsymbol{B}' = \begin{bmatrix} b_{11} & 0 \\ 0 & 0 \\ 0 & e_4 \end{bmatrix} \tag{30b}$$

$$\boldsymbol{C}' = \begin{bmatrix} c_{11} & c_{12} & d_{12} \\ c_{21} & c_{22} & d_{22} \\ 0 & 0 & 1 \end{bmatrix} \tag{30c}$$

$$\boldsymbol{D}' = [0] \tag{30d}$$

The various T_{sp} values are obtained by Equations (30) for each cell. After T_{sp} values are calculated for all cells in each step, these values are averaged and the averaged values is used T_{sp} of next step. This averaging means the approximation that any part of battery pack housing have the exact the same temperature. To increase the fidelity of the model, cell to cell heat transportation needs to be considered. However, in the case of a small battery pack, the temperature distribution is relatively small [11] and the system, including cell to cell heat transportation, should be described as a set of ordinary differential equations. Therefore in order to achieve fast calculation, the temperature distribution in the battery pack and battery housing is regarded as negligible in this model.

2. 3 Aging model

The aging model consists of both calendar and cycle aging models. The battery degradation model considered cell temperature, open circuit voltage: $V_{oc,}$ and depth of discharge: ΔDOD was reported by Smith et al.[7],[12].The remarkable point of their model is that both calendar and cycle fade as well as both capacity and impedance fade were expressed in one model. The impedance fade of the model is described as the sum of Li ion reduction due to SEI growth factor and active material site loss factors. Meanwhile, the capacity fade of this model is described as the maximum value of Li ion reduction or active material site loss. The stress factor of the battery cell’s temperature, V_{oc} and ΔDOD is expressed by Arrhenius, Tafel and Wöhler dependence, respectively. Wöhler dependence is a kind of relationship utilized to describe material fatigue by cycle stresses [13]. The cycle number where the material is destroyed is a function of stress amplitude. This dependence has been utilized to assess the potential for crack nucleation of active material particles due to ΔDOD [8]. The stress of active material surfaces is also affected by C-rate [14] and is related to capacity degradation by cycle tests [15]. Therefore effect of both ΔDOD and C-rate on cycle fade are unified in the one Wöhler dependence equation in this work. As mentioned in Section 2.1, the equivalent circuit of our model has three resistances and two capacitance. Therefore degradation of all components should be defined. As for calendar fade, it is reported that battery cells preserved 33 months without any measurement have very little change except ohmic resistance[16]. Thus, calendar degradation except R_{zs} are ignored in this model. On the contrary, as for cycle fade, all components increase with increasing ohmic resistance[17][18]. Therefore, the R_{zs} degradation is defined by the results of cycle test and other components of the equivalent circuit are defined as a proportion of cycle degradation of R_{zs}. To deal with a battery pack which has R_{zs} and CAP_{cell} distribution, the degradation amount of each cell should be defined as a proportion of the initial value or just adding functions of stress factors. According to the cycle life measurement of eight SONY 18650 cells [19], the increasing amount of impedance seems independent with different initial resistance values. Meanwhile, as for increase in the amount of capacity, the definition described in literature [7] which mentioned the reduction amount of capacity by cycle fade is a proportion of the initial amount of capacity is applied. Accordingly, the R_{zs} and CAP_{cell} distribution of this model is defined as

$$R_{zs}(\tau)_{\tau=t} \equiv R_{zs,t} = R_{zs,0} + \theta_{ref,R1}\theta_{T_{cc},R}\theta_{V_{oc},R1}\tau^{\frac{1}{2}} + \theta_{ref,R2}\theta_{V_{oc},R2}\theta_{\Delta DOD-C,R}\nu \tag{31a}$$

$$CAP_{cell}(\tau)_{\tau=t} \equiv CAP_{cell,t} = CAP_{cell,0}\left\{1 - \frac{1}{CAP_{cell,0\_nominal}}\left(\theta_{ref,C1}\theta_{T_{cc},C}\theta_{V_{oc},C1}\tau^{\frac{1}{2}} + \theta_{ref,C2}\theta_{V_{oc},C2}\theta_{\Delta DOD-C,C}\nu\right)\right\} \tag{31b}$$

Where

$$\theta_{T_{cc},l} = exp\left\{\frac{-E_{al}}{\mathcal{R}_{ug}}\left(\frac{1}{T_{cc}} - \frac{1}{T_{cc,ref}}\right)\right\} \quad (l = R \text{ or } C) \tag{32a}$$

$$\theta_{V_{oc},l} = exp\left\{\frac{\beta_l F}{\mathcal{R}_{ug}}\left(\frac{V_{oc}}{T_{cc}} - \frac{V_{oc,ref}}{T_{cc,ref}}\right)\right\} \quad (l = R1, R2, C1 \text{ or } C2) \tag{32b}$$

$$\theta_{\Delta DOD-C,l} = \left(\frac{\Delta DOD_i + \phi_l C - rate_i}{\Delta DOD_{ref} + C - rate_{ref}}\right)^{\eta_l} \quad (l = R \text{ or } C) \tag{32c}$$

where $\theta_{T_{cc},l}$ shows the Arrhenius dependence on cell temperature. In this model we use T_{cc} as representative value of the cell temperature. As the viewpoint of safer design, this is an appropriate value because the high temperature proceed to battery cell degradation. $\theta_{V_{oc},l}$ shows the Tafel dependence on V_{oc} and $\theta_{\Delta DOD-C,l}$ shows the Wöhler dependence on ΔDOD and $C - rate_i$ in one cycle. The relationship between ΔDOD_i and $C - rate_i$ are described as a simple linear combination. In Equations (32) $\theta_{ref,l}$, E_{al}, β_l, η_l and ϕ_l are fitting parameters, $\mathcal{R}_{ug}$ and F are the universal gas constant and Faraday constant, respectively. $CAP_{cell,nominal}$ is the initial capacity of the cell which is used for parameter acquisition. ν is the cycle number when time is t . $T_{cc,ref}$, $V_{oc,ref}$, ΔDOD_{ref} and $C - rate_{ref}$ are arbitrary constants for convenience of calculation. As mentioned in Section 1, the value of ΔDOD_i and $C - rate_i$ are strongly correlated with stress on active materials [8],[14]. In addition, the strain on active material particles monotonically increases with increasing stress [20],[21]. Therefore, the value of $\Delta DOD_i + \phi_l C - rate_i$ is regarded as a proportion of strain on the active material in this model. The Rainflow method [9],[22] which is a popular method to evaluate material damage by random stress from strain-elapsed time curves can be adapted to battery degradation estimation under this assumption. To adapt to a real-time arbitrary system, $R_{zs,t}$ and $CAP_{cell,t}$ can be expanded from Equations (33) and (34) as

$$R_{zs,t} = R_{zs,0} + \psi_{cal,R,t} + \psi_{cyc,R} \tag{33a}$$

$$CAP_{cell,t} = CAP_{cell,0}\left\{1 - \frac{1}{CAP_{cell,0_{nominal}}}\left(\psi_{cal,C,t} + \psi_{cyc,C}\right)\right\} \tag{33b}$$

where the values of ψ are the degradation amount of $R_{zs,t}$ and $CAP_{cell,t}$ by calendar factor and cycle factors. The calendar degradation factor are easily described as

$$\psi_{cal,R,t} = -\theta_{ref,R1}\int_0^t \theta_{T_{cc},R}\theta_{V_{oc},R1}\frac{1}{\sqrt{2}}\tau^{-\frac{1}{2}}d\tau \cong \theta_{ref,R1}\sum_{k=-(n-1)}^{0}\theta_{T_{cc},R,t+k\Delta t}\theta_{V_{oc},R1,t+k\Delta t}\left\{(t+k\Delta t)^{\frac{1}{2}} - (t+(k-1)\Delta t)^{\frac{1}{2}}\right\} \tag{34a}$$

$$\psi_{cal,C,t} = -\theta_{ref,C1}\int_0^t \theta_{T_{cc},C}\theta_{V_{oc},C1}\frac{1}{\sqrt{2}}\tau^{-\frac{1}{2}}d\tau \cong \theta_{ref,C1}\sum_{k=-(n-1)}^{0}\theta_{T_{cc},C,t+k\Delta t}\theta_{V_{oc},C1,t+k\Delta t}\left\{(t+k\Delta t)^{\frac{1}{2}} - (t+(k-1)\Delta t)^{\frac{1}{2}}\right\} \tag{34b}$$

Cycle degradation factors in Equations (34) are calculated by the algorithm of the Rainflow method. The flow chart of the algorithm is shown in Figure 3. The Rainflow list shown in Figure 3 is a kind of the look up table which records the essential information for cycle fade calculations. In addition, the algorithm have the Unchanged value: a_{uc} which is the cycle degradation value calculated by previous time step. the cycle degradation is expressed by the sum of a_{uc} and the value calculated by the Rainflow list. $\theta_{\Delta DOD-C}$ and t_{pv} indicate the difference of $\Delta DOD + \phi_l C - rate$ and time between peak to valley of time versus $\Delta DOD_i + \phi_l C - rate_i$ curve. $\overline{\theta_{V_{oc}}}$ is the

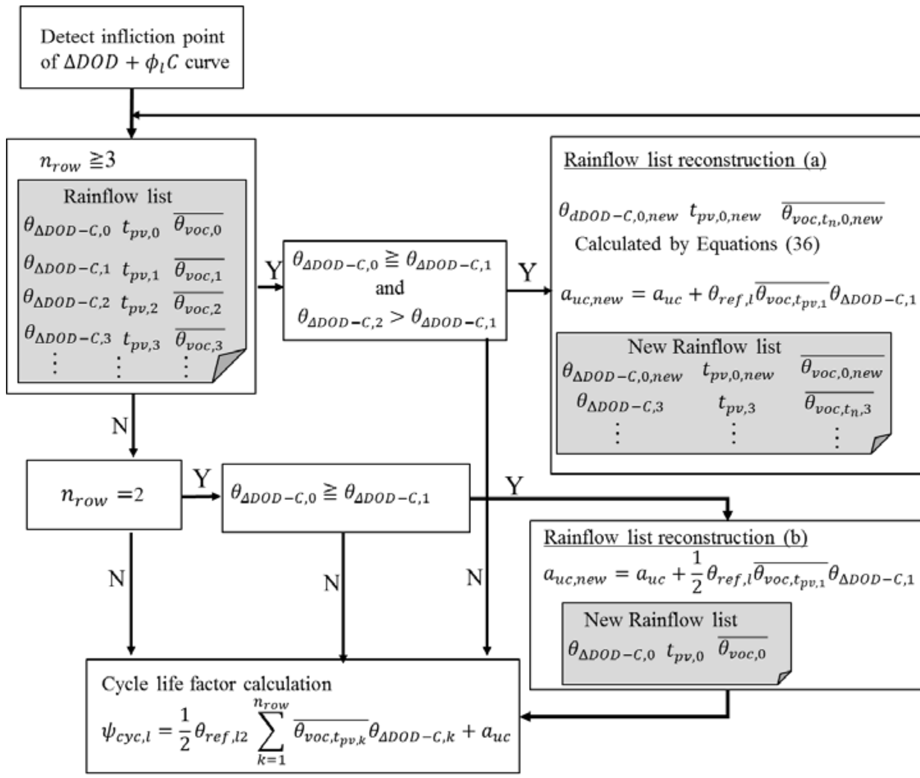

Figure 3. The flow chart of the Rainflow algorism for calculate cycle aging of capacity and impedance.

normalized value of the $\theta_{V_{oc},R2}$ or $\theta_{V_{oc},C2}$ described as Equations (35).

$$\overline{\theta_{V_{oc}}} = \frac{1}{t_{pv,k}}\int_{\mathcal{T}_{k-1}}^{\mathcal{T}_k}\theta_{V_{oc}}d\tau \quad (35a)$$

$$\mathcal{T}_k = \sum_{l=1}^{k} t_{pv,l} \quad (35b)$$

The model detect the infliction point of the $\Delta DOD + \phi_l C$ curve, $\theta_{\Delta DOD-C}$, t_{pv} and $\overline{\theta_{V_{oc}}}$ are recorded at the top of the Rainflow list as $\theta_{\Delta DOD-C,0}$, $t_{pv,0}$ and $\overline{\theta_{V_{oc},0}}$.

The Rainflow list is reconstructed (Rainflow list reconstruction (a) in Figure 3) when the $\theta_{\Delta DOD-C}$ match two conditions as follows. The first condition is that $n_{row} \geqq 3$ as well as $\theta_{\Delta DOD-C,0} \geqq \theta_{dDOD-C,1}$ and $\theta_{\Delta DOD-C,2} > \theta_{dDOD-C,1}$. $\theta_{\Delta DOD-C,0,new}$, $t_{pv,0,new}$ and $\theta_{voc,t_n,0,new}$ are calculated by Equations (36). The subscript new shows the newest calculated values in the first row of the Rainflow list and Unchangeable values.

$$\theta_{\Delta DOD-C,0,new} = \theta_{\Delta DOD-C,0} + \theta_{\Delta DOD-C,2} - \theta_{\Delta DOD-C,1} \quad (36a)$$

$$t_{pv,0,new} = t_{pv,0} + t_{pv,1} + t_{pv,2} \quad (36b)$$

$$\overline{\theta_{voc,0,new}} = \frac{t_{pv,0}\overline{\theta_{voc,0}} + t_{pv,1}\overline{\theta_{voc,1}} + t_{pv,2}\overline{\theta_{voc,2}}}{t_{pv,0,new}} \quad (36c)$$

where $t_{p,k}$ is the time at the kth inflection point of time versus $\Delta DOD_i + \phi_l C - rate_i$ curve. Moreover, the first 3 rows of the list are deleted and $\theta_{ref,l}\overline{\theta_{voc,t_{pv,1}}}\theta_{\Delta DOD-C,1}$ is added to a_{uc}. If the reconstructed list have more than three rows, the model repeat the same process.

If the $n_{row} = 2$ as well as $\theta_{\Delta DOD-C,0} \geqq \theta_{dDOD-C,1}$, the Rainflow list is also reconstructed. The second row of the Rainflow list is deleted and $0.5\theta_{ref,l}\overline{\theta_{voc,t_{pv,1}}}\theta_{\Delta DOD-C,1}$ is added to a_{uc}.

The other cases, The cycle degradation $\psi_{cyc,l}$ is expressed as

$$\psi_{cyc,l} = \frac{1}{2}\theta_{ref,l2}\sum_{k=1}^{n_{row}}\overline{\theta_{voc,t_{pv,k}}}\theta_{\Delta DOD-C,k} + a_{uc} \quad (l = R \text{ or } C) \quad (37)$$

The value of $\psi_{cyc,l}$ is only renewed when the model detect the infliction point of the $\Delta DOD + \phi_l C$ curve, the other time steps, the value is the same as previous time step.

3 Parameter Acquisition

In this section, parameters acquisition for the model is presented. As for the electrical model, V_{oc} and equivalent circuit components, which are as the functions of SoC and temperature of the battery cell, is estimated by the fitting of reported test data for the 2.37Ah Molicel 18650 cells[23]. The thermal model parameters are estimated by material constants of Molicel 18650 cells [10] and the geometry of the BB-2590 battery pack. The parameters for the aging model are estimated by using 1.4Ah SONY 18650 cell data because they have the same $LiCoO_2$/carbon chemistry and plenty of experimental data was reported[24]-[26].

3.1 Electrical and Thermal model

The function $V_{oc}(SoC)$ is estimated by SoC-V_{oc} curve of 2.37Ah Molicel 18650 cells [23].
This curve is fitted by

$$\begin{aligned} V_{oc}(SoC) = K_0 + K_1 \frac{1}{1+e^{L_1(SoC-M_1)}} + K_2 \frac{1}{1+e^{L_2(SoC-M_2)}} \\ + K_3 \frac{1}{1+e^{L_3(SoC-1)}} + K_4 \frac{1}{1+e^{LSoC}} + K_5 SoC \\ - e^{L_5(soc-M_3)} + e^{L_6(SoC-M_4)} \end{aligned} \quad (38)$$

Equation (38) is based on the fitting formula reported by Weng et al [24]. The fitting result is shown as Figure 4. The seventh and eighth terms of Equation (38) is added to original formula to reduce fitting error of V_{oc} especially near SoC = 0 and 1 area. The average and maximum fitting error is 4.5mV and 21mV, respectively.
The coefficients $K_{1-5,}$ $L_{1-6,}$ $M_{1-4,}$ are obtained by the least-square method. The 6th and 7th term of this fitting curve are added.
The functions $R_{zs}(T_{cc})$, $R_{z1}(SoC, T_{cc})$, $R_{z2}(SoC, T_{cc})$, $C_{z1}(SoC, T_{cc})$and $C_{z2}(SoC, T_{cc})$are estimated by the product of resistance and capacitance versus SoC curve measured under various temperature[23]. The reported fitting function for a cylindrical battery [1] is adapted to use this estimation. The function is shown as Equations (39)

$$R_{zs} = R_{0,R_{zs}} exp\left(\frac{T_{ref,R_{zs}}}{T_{cc} - T_{shift,R_{zs}}}\right) \quad (39a)$$

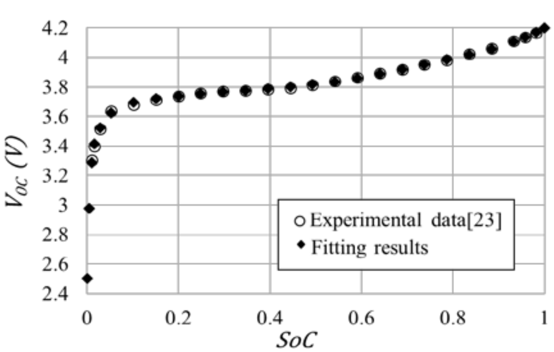

Figure 4. SoC -V_{oc} measurement data of [23] and fitting curve calculated by Eq. (38).

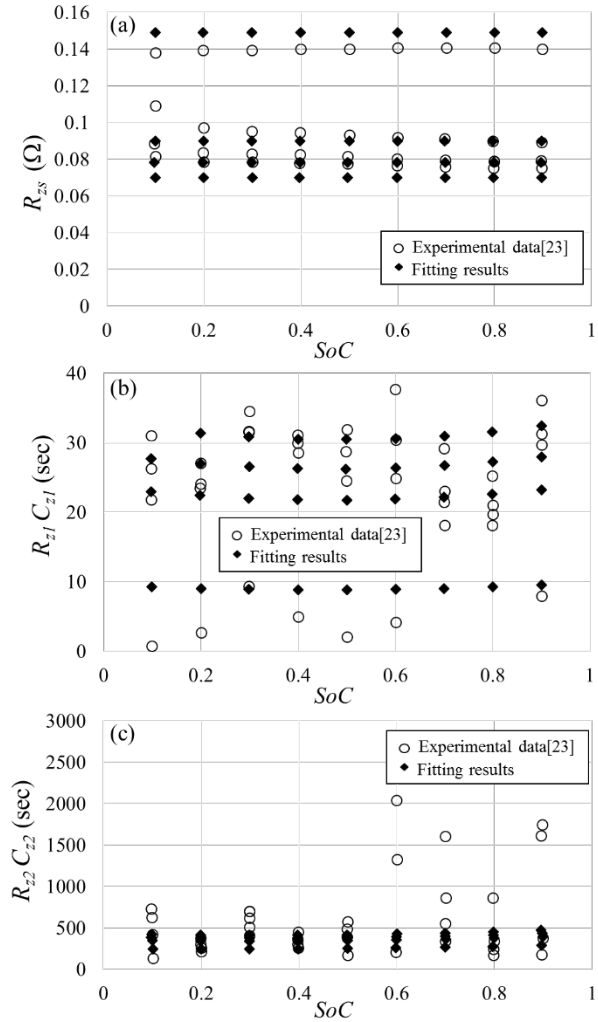

Figure 5. Electric components of the equivalent circuit estimated by the measurement data [23] and fitting curve calculated by eqs. (38). (a) R_{zs}, (b) R_{z1} and C_{z1} and (c) R_{z2} and C_{z2},

Table 1. Parameters used thermal model

Length of a battery cell (m)	0.0652
Radius of a battery cell: r (m)	0.0092
Effective heat transfer coefficient out of cells: h (W/m2/K)	22
Cell heat conductivity: k_t (W/m/K)	3.4
Cell density: ρ (kg/m3)	2747
Cell Specific heat coefficient: $C_{p,cell}$ (J/kg/K)	1280
Pack valid cooling area (m2)	0.0349
Pack housing heat conductivity (W/m/K)	0.25
Pack housing thickness (m)	0.001
Pack around air thermal coefficient (W/m2/K)	10
Pack heat capacity: C_{pack} (J/K)	185.8

Figure 6. Situation of embedded BB-2590 batteries. (Yellow boxes between wheels)

$$R_{zl} = (R_{0,R_{zl}} + D_{1,zl}SOC + D_{2,zl}SOC^2)exp\left(\frac{T_{ref,R_{zl}}}{T_{cc} - T_{shift,R_{zl}}}\right) \quad (l = 1\ or\ 2) \qquad (39b)$$

$$C_{zl} = (C_{0,R_{zl}} + D_{3,zl}SOC + D_{4,zl}SOC^2) + (D_{5,zl} + D_{6,zl}SOC + D_{7,zl}SOC^2)T_{cc}, \quad (l = 1\ or\ 2) \qquad (39c)$$

where $T_{ref}, T_{shift}, R_0, C_0$ and $D_{1-7,zl}$ are fitting parameters. The fitting results are shown in Figure 5(a), (b) and (c).

As for the thermal model, the parameters are defined in Table 1. In this work, we assumed the embedded batteries on the iRobot Pack-bot are as shown in Figure 6. As the picture shows, the battery is connected to power outlet by one smallest plain and fixed the chassis by the one largest plain. Therefore, the model has two thermal insulated walls and four air cooling surface. This means the generated heat from a battery cell can dissipate limited surface of the battery pack.

3.2 Aging model

The 1.4Ah SONY 18650 cells data [24]-[26] are fitted by equations (32) and (33). The fitted data is shown in Figure 7.

The fitting for the calendar life curve partially agrees with the experimental data. However, the fitting for the cycle test data is less accurate. One possibility of this error is the lack of measurement and time information. Electrical measurements such as capacity measurement to the battery often affect the cycle degradation. Moreover the time interval between cycles causes calendar fade.

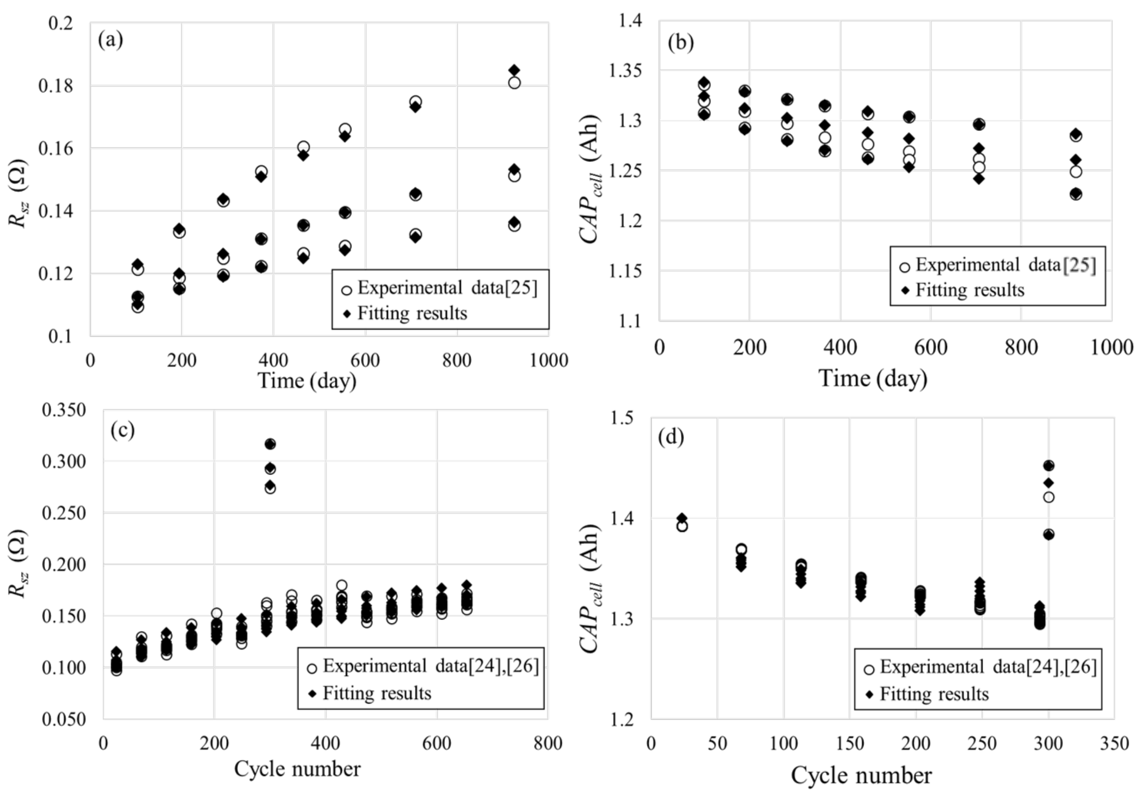

Figure 7. The degradation data of 18650 type SONY 1.4Ah battery with data $LiCoO_2$/carbon chemistry [24]-[26] and fitting curve calculated by equations mentioned in Section 2.3. Figure 5(a) and (b) show the measurement data of calendar life data. Figure 5(c) and (b) shows the measurement data of cycle test data.

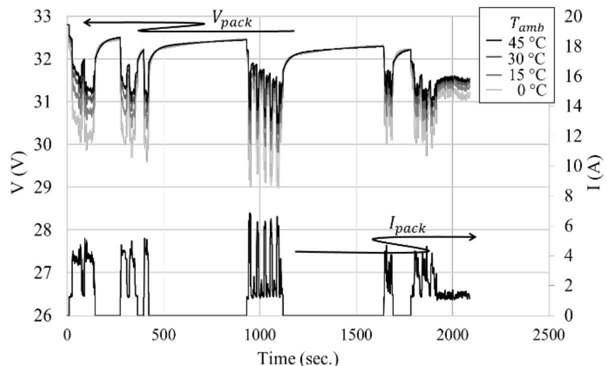

Figure 8. Calculated voltage profile of an on-board BB-2590 battery under various ambient temperature conditions.

4. Results and Discussions

In this section, the results of the simulation model are demonstrated. In all simulation, I_{leak}, R_{zs} and CAP_{cell} of cells have distributions. The average value of I_{leak} is 0.0074 mA and the value have 1% distribution within 6σ. R_{zs} have also 1.3% distribution within 6σ. The average value of CAP_{cell} is 2.37Ah and the value have 0.5% distribution within 3σ. These values are estimated by the experimental results and catalog specification In section 4.1, the voltage and temperature profiles are simulated under various T_{amb} conditions. In section 4.2, the simulation results of simple calendar life and cycle life tests are shown.

4.1 Capability Simulation

The voltage profile of the on-board BB-2590 battery pack model under various T_{amb} is shown in Figure 8. The model battery pack was brand-new before starting this simulation. The electrical current, which is the input data of this simulation, is measured by certain Pack-bot driving data on various terrains such as pea gravel, sand, crushed concrete and hill. The pack SoC changes from 0.93 to 0.85 in this profile. The data seems appropriate qualitatively. For instance, the voltage drop amount increases with decreasing T_{amb} due to high R_{zs} at low temperature as shown in Figure 5(a). Moreover, the peak of the voltage drop amount at around 1000 seconds of this profile decreases from 26V to 25V due to voltage drop of the RC pair in the equivalent circuit.

The temperature profile of the battery pack and a typical cell are shown in Figure 9. These profiles seem reasonable. The increase in the rate of temperature by electric current increases with decreasing T_{amb} . In the case where T_{amb} is low, the Joule heat from the battery increases due to high impedance. T_{cc} and T_{sc} values are very similar in this model. The heat conductivity of $LiCoO_2$ is as high as 3.4 W/K/m[27], fives times larger than the heat conductivity of $LiFePO_4$ [10]. Moreover, strictly speaking, the T_{sc} value is not the real battery cell surface covered can or

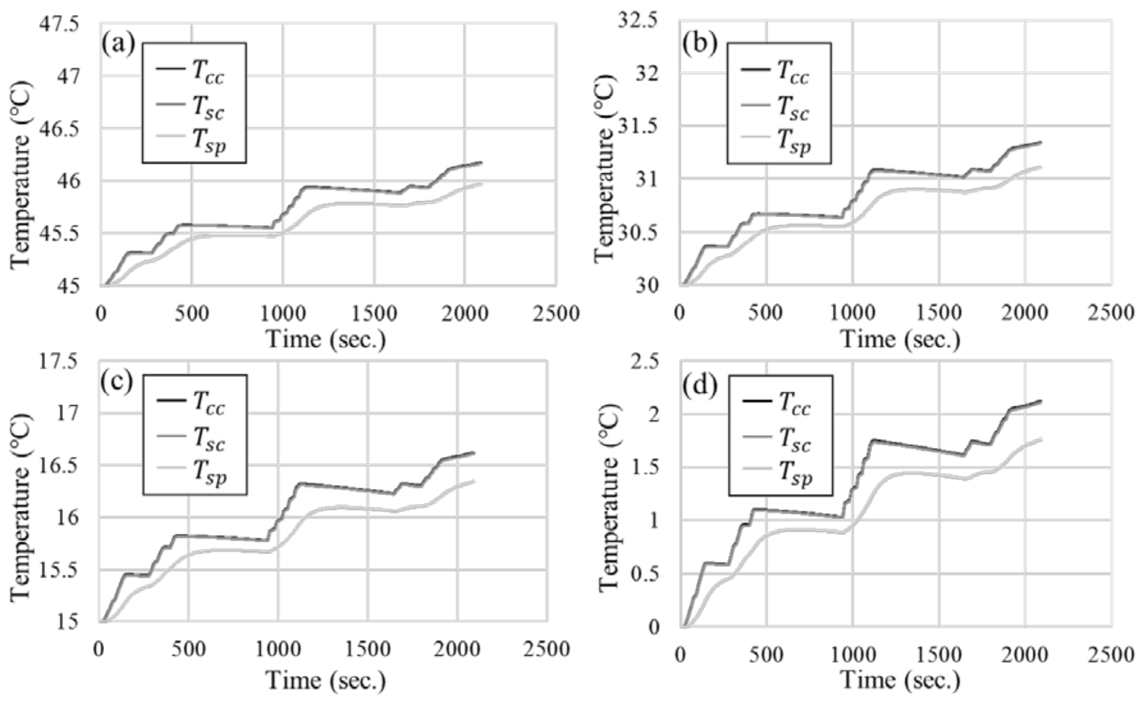

Figure 9. Calculated temperature profile of an on-board BB-2590 battery pack and its typical battery cell under various ambient temperature conditions. (a) T_{amb} =45°C; (b) T_{amb} =30°C; (c) T_{amb} =15°C; (d) T_{amb} =0°C.

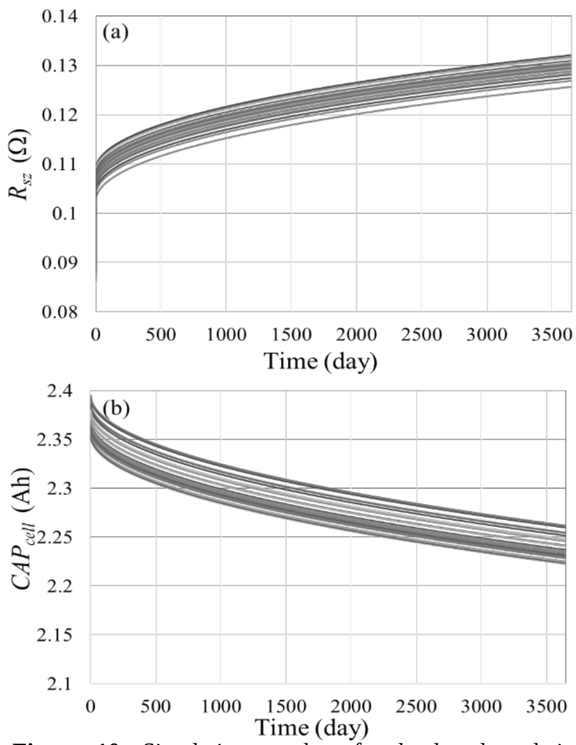

Figure 10. Simulation results of calendar degradation estimation. Each line shows degradation of each cell in a battery pack. (a) ohmic resistance; (b) capacity of cells.

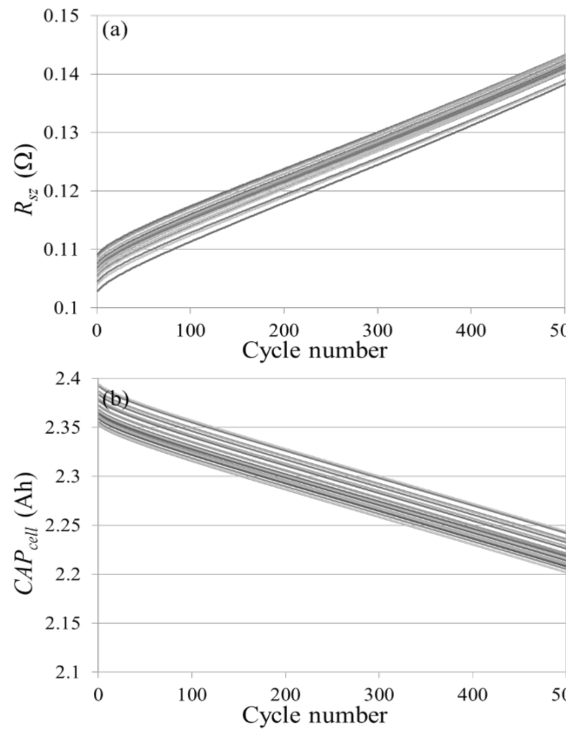

Figure 11. Simulation results of cycle degradation estimation. Each line shows degradation of each cell in a battery pack. (a) ohmic resistance; (b) capacity of cells.

pack but the surface of the jelly roll. Accordingly, the T_{cc} and T_{sc} in the results of this simulation are the almost the same value.

4.2 Life span order simulation

The battery model utilized in the lifespan test also assumes an onboard BB-2590 battery pack reported in [19] and [28]. Both calculations are conducted under the simulated 15 °C ambient temperature. The resistance and capacity degradation in Figure 10 is much lower than Figure 7 because the ambient temperature of the calendar fade data shown in Figure 7 are conducted as high as 40,50 and 60°C. The tendency of fade amount and tendency seems roughly reasonable. The distribution of cell capacity slightly decreases as time proceed from 0.238% to 0.224%. On the other hand, the distribution of cell capacity is almost the same as far as this simulation (<10^{-5}% order). The total calculation time is as short as 58 hours. This calculation time is 0.07% of the real time.

The simulation results of cycle aging is shown as Figure 11. The total cycle number is 500 times and elapsed time is 250 days. A cycle consists of a two-hours "discharge phase" (2.6A discharging), and a ten-hours "CCCV phase" (charging under CC-CV program). The discharging current, 2.6A is the average of a robot operation on the various terrain [29]. During the CCCV phase, at first the battery pack is charged at a 1A . When the battery pack voltage reaches 4.1V, electric current is decreased. At last, when the charging current reach 50mV, the current is turned off. The result of the simulation seems natural as well as calendar life data. The distribution of cell capacity slightly increases from 0.238% to 0.241% in 500 cycles. This tendency is opposite tendency compared with the calender life simulation. The distribution of ohmic resistrance decreases from 0.278% to 0.249%. The total calculation time is as short as 32 hours. This calculation time is 0.55% of the real time. Those simulation results have a room for improving by the measurement results of basic data such as HPPC or cycle test data under various conditions and should be validated by experimental data.

5. Conclusion

A semi-empirical model for predicting capability and life span of small size Li ion battery packs is established in this work. The model consists of a simple BMS model, existing electro-thermal model, and calendar and cycle aging models. Moreover the capability and life span data of BB-2590 battery packs which are embedded on the packbot were obtained. All simulation results seem reasonable and the calculation time is short enough to be real-time. The next step is evaluating the model using actual experimental data. Once the model is fully validated, the algorithm will be useful for design and development of small battery packs for UGVs.

References

[1] X. Lin, H. E. Perez, S. Mohan, J. B. Siegel, A. G. Stefanopoulou, Y. Ding and M. P. Castanier, "*A lumped-parameter electro-thermal model for cylindrical batteries*" Journal of Power Sources 257 (2014) 1-11.

[2] X. Lin, H. E. Perez1, J. B. Siegel, A. G. Stefanopoulou, Y. Ding and M. P. Castanier, "*Parameterization and Observability Analysis of Scalable Battery Clusters for Onboard Thermal Management*" RHEVE 2011 6-7 December 2011 – Proceedings.

[3] P. Ramadass, B. Haran, R. White and B. N. Popov, "*Mathematical modeling of the capacity fade of Li-ion cells*", Journal of Power Sources 123 (2003) 230–240.

[4] B. J. Yurkovich, "*Electrothermal Battery Pack Modeling and Simulation*" Master Thesis in the Graduate School of The Ohio State University. (2010).

[5] A. Cordoba-Arenas, S. Onori b, 1, Y. Guezennec and G. Rizzoni, "*Capacity and power fade cycle-life model for plug-in hybrid electric vehicle lithium-ion battery cells containing blended spinel and layered-oxide positive electrodes*", Journal of Power Sources 278 (2015) 473-483.

[6] A. Cordoba-Arenas, S. Onori, G. Rizzoni, "*A control-oriented lithium-ion battery pack model for plug-in hybrid electric vehicle cycle-life studies and system design with consideration of health management*" Journal of Power Sources 279 (2015) 1-18.

[7] K. Smith, M. Earleywine, E. Wood and A. Pesaran, "*Battery wear from disparate duty-cycles: Opportunities for electric-drive vehicle battery health management*" Preprint of the 2012 American Control Conference, June 27–29, (2012).

[8] M. W. Verbrugge, and Y.-T. Cheng, "*Stress and Strain-Energy Distributions within Diffusion-Controlled Insertion-Electrode Particles Subjected to Periodic Potential Excitations*", Journal of The Electrochemical Society, 156 (2009) A927-A937.

[9] T. Endo and H. Anzai, "*Refined Rainflow Algorithm: P/V Difference Method*", Journal of the Society of Materials Science, Japan 30 (1981) 89-93.

[10]Y. Kim, "*Power Capability Estimation Accounting for Thermal AND Electrical Constants of Lithium-Ion Batteries*" Doctorate Thesis in the Graduate School of University of Michigan. (2014).

[11] K. Yeow, H. Teng, M. Thellieza and E. Tan, "*3D Thermal Analysis of Li-ion Battery Cells with Various Geometries and Cooling Conditions Using Abaqus*" in Proceedings of the SIMULIA Community Conference, Providence, RI, USA, May (2012).

[12] K. Smith, J. Neubauer, E. Wood, M. Jun and A. Pesaran, "*Models for Battery Reliability and Lifetime Applications in Design and Health Management*", Presentation material for Battery Congress, April 15-16, (2013).

[13] A. Wöhler,. "*Über die Festigkeitsversuche mit Eisen und Stahl, Zeitschrift für Bauwesen*" 20 (1870)73-106

[14] X. Zhang, W. Shyy and A. M. Sastrya, "*Numerical Simulation of Intercalation-Induced Stress in Li-Ion Battery Electrode Particles*" Journal of The Electrochemical Society, 154 (2007) A910-A916.

[15] L. Serrao, S. Onori, A. Sciarretta, Y. Guezennec and G. Rizzoni, "*Optimal energy management of hybrid electric vehicles including battery aging*", 2011 American Control Conference June 29 - July 01, 2011, San Francisco, CA, USA,

[16] M. C. Smart, K. B. Chin, L. D. Whitcanack and B. V. Ratnakumar,"*Storage Characteristics of Li-Ion Batteries*", presentation material of NASA Battery November 14-16, (2006).

[17] U. Tröltzsch, O. Kanoun and H.-R. Tränkler, "*Characterizing aging effects of lithium ion batteries by impedance spectroscopy*", Electrochimica Acta 51 (2006) 1664–1672

[18] N. Kakimoto and K. Goto, "*Capacity-Fading Model of Lithium-Ion Battery Applicable to Multicell Storage Systems*", IEEE Transactions on Sustainable Energy, 7(2016) 108-117

[19] A. H. Zimmerman and M. V. Quinzio, "*Performance of SONY 18650-HC Lithium-Ion Cells for Various Cycling Rates*" AEROSPACE REPORT NO.TR-2010(8550)-5, (2010).

[20] Jun Xu, Binghe Liu and Dayong Hu, "*State of Charge Dependent Mechanical Integrity Behavior of 18650 Lithium-ion Batteries*"Scientific Reports 6, (2016) Article number: 21829.

[21] Y. Li, X. Chenga, Y. Zhang, "First-principle Analyses of Stress and Strain during Li Deintercalation in $LiCoO_2$" ECS Transactions, 19 (2009) 1-9

[22] "*Standard practices for Cycle Counting Fatigue Analysis*" ASTM E 1049-1085, (2005)

[23] Y. Kim, S. Mohan, A. Stefanopoulou, J. Siegel, Y. Ding, M. Castanier, D. Anderson and Y. Li, "*Electro-thermal Cylindrical Battery Model for Robotic Packs*", Presentation materials for ARC Collaborative Research Seminar Series Winter 2013.

[24] C. Weng, J. Sun, H. Peng, "*A unified open-circuit-voltage model of lithium-ion batteries for state-of-charge estimation and state-of-health monitoring*", Journal of Power Sources 258 (2014) 228-237.

[25] G. Ning, B. Haran and B. N. Popov, "*Capacity Fade Study of Lithium-ion Battery Cycled at High Discharge Rates*", Journal of Power Sources 117, (2003) 160–169

[26] G. Dudley, "*High Temperature Testing of Lithium-Ion Batteries for BepiColombo Orbiters (February 2005 update)*" Presentation material for BepiColombo TDA February 23. (2005).

[27] H. Maleki, S. A. Hallaj, J. Robert Selman, R. B. Dinwiddie and H. Wang. "*Thermal Properties of Lithium-Ion Battery and Components*", Journal of The Electrochemical Society, 146 (1999) 947-954

[28] Molicel co. "*MODEL ICR18650J Product Data Sheet*".

[29] K. Boice, A. Leo, J. Lee J. Paulson, Jr., M. Skalny and T. Valascho, "*Baseline Field Testing of BB-2590 Lithium-Ion Batteries using an iRobot FasTac 510 Robot*", TARDEC technical report (2010) No. 213